

First results with the ORPHEUS dark matter detector

K. Borer, G. Czapek, F. Hasenbalg, M. Hauser, S. Janos,
P. Loaiza, U. Moser, K. Pretzl*, C. Schütz, P. Wicht,
and S. Wüthrich

*Laboratory for High Energy Physics, University of Bern, Sidlerstrasse 5, CH 3012
Bern, Switzerland*

Abstract

The ORPHEUS dark matter detector is operating at our underground laboratory in Bern (70 m.w.e.). The detector relies on measuring the magnetic flux variation produced by weakly interacting massive particles (WIMPs) as they heat micron-sized superheated superconducting tin granules (SSG) and induce superconducting-to-normal phase transitions. In an initial phase, 0.45 kg of tin granules in a segmented detector volume have been used. In this paper a general description of the experimental set-up, overall performance of the detector, and first results are presented.

Key words: cold dark matter, direct detection, cryogenic detectors

PACS: 95.35.+d, 14.80.Ly, 07.20.Mc

* Corresponding author. Tel.: +41-31-631-8566; fax: +41-31-631-4487.

E-mail address: klaus.pretzl@lhcp.unibe.ch (K. Pretzl).

1 Introduction

According to the latest cosmic microwave background measurements [1] combined with other cosmological observations [2,3,4,5,6], the matter density of the universe comprises 27% (for a Hubble constant $H_0 = 71 \text{ km s}^{-1} \text{ Mpc}^{-1}$) of the critical density while the remaining 73% is in the form of a cosmological constant of an unknown nature. With only $\approx 4\%$ of the matter density in the form of baryons, the rest should be of some exotic non-baryonic nature. This non-luminous and non-relativistic matter, known as cold dark matter, constitutes an essential ingredient in theories of structure formation in the universe. From the class of candidates for cold dark matter generically known as weakly interacting massive particles (WIMPs), the lightest supersymmetric particle, the neutralino [7], seems to be the most promising. The upper bound for the mass of the neutralino in the constrained minimal supersymmetric extension of the Standard Model is 500 GeV [8], its lower bound of 46 GeV comes from e^+e^- collider experiments [9].

The ORPHEUS project is a direct search experiment looking for cold dark matter aiming at detecting the small energy deposited by a neutralino after being elastically scattered off a target nucleus [10]. The detector consists of a homogeneous mixture of superheated superconducting tin granules (SSG) embedded in a dielectric filling material and exposed to an external magnetic field. The type I superconducting granules are kept slightly below the boundary of their superconducting-to-normal phase transition in a metastable state. The recoil energy released by a particle interacting with a granule causes a temperature increase inversely proportional to the specific heat of the granule. Due to the small value of the specific heat at low temperatures, the deposited energy is enough to make a granule normal-conducting. A 1 keV energy deposition in a granule of 35 μm diameter at a bath temperature of 110 mK increases the temperature of the granule by typically 100 mK. The induced flux change (*flip*) due to the disappearance of the Meissner-Ochsenfeld effect is measured by an RLC circuit. A general description of SSG detectors is given in Refs. [11,12,13].

This paper is organised as follows: section 2 describes the experimental setup, the shielding, and the data acquisition system; section 3 describes the data taking and its reduction procedure as well as the detector response to muons, section 4 outlines the main results of this experiment and presents the inferred exclusion plot. Finally, section 5 discusses possible improvements of the detector capabilities and outlook. An appendix briefly describes how the expected rates in our detector are computed.

2 Experimental setup

ORPHEUS is located in the underground facility of the University of Bern (70 m.w.e.). A scheme of the experimental setup is shown in Fig. 1. It consists of the detector chamber, the electronic readout, the cryogenic system, the passive shielding, and the muon veto. Each part is described in some detail below.

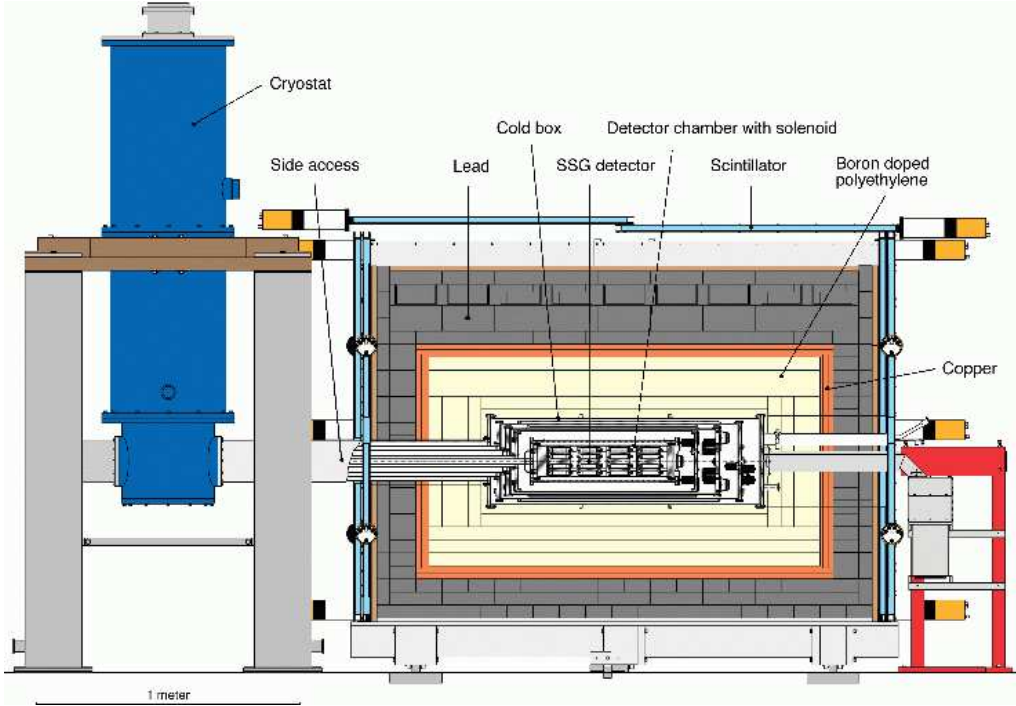


Fig. 1. ORPHEUS experimental setup.

2.1 SSG detector and detector chamber

Tin granules, of 5N purity, with two different diameter ranges are selected as sensitive material. The granules are produced by the Technical University of Clausthal using a fine powder gas atomisation technique and sieved in Bern to the desired diameter ranges. Out of 50 kg of granules of different sizes only ≈ 1 kg remain after sieving. A sample of granules of both diameter ranges was measured with an optical scanning microscope. The sample of large granules was found to have a nearly Gaussian distribution with a mean diameter $\hat{\phi} = 36.6 \mu\text{m}$ and a standard deviation of $\sigma = 2.2 \mu\text{m}$. The sample of small granules also exhibited a Gaussian distribution but with a mean diameter $\hat{\phi} = 27.7 \mu\text{m}$ and $\sigma = 4.1 \mu\text{m}$. To avoid magnetic interactions among the granules, we use Teflon powder as a filling material at a volume filling factor for tin of 10%. This corresponds roughly to a mean distance between

the granule centres of about 2 granule diameters.

The detector chamber consists of 56 pick-up coils filled with sensitive material. The coils, 1.8 cm in diameter (1.6 cm inner diameter), 6.8 cm long and with roughly 1500 windings, were filled half of them with large granules and the other half with small ones. A filled coil contains ≈ 8 g of tin. A total mass of 207 g was measured for the large granules (excluding 2 dead channels) and 215 g for the small ones (excluding 1 dead channel). The dead channels were due to wiring problems at the pick-up coil and register no output signal. Inside the chamber 4 detector modules made of Delrin, serve as a holder for the pick-up coils with 14 coils in each module. A test coil with 10 windings around every detector module generates a test signal. Fig. 2 shows the detector chamber with the four modules and the superconducting solenoid surrounding it. This configuration provides a highly segmented detector which is very useful to locate hot spots and to reject spurious events.

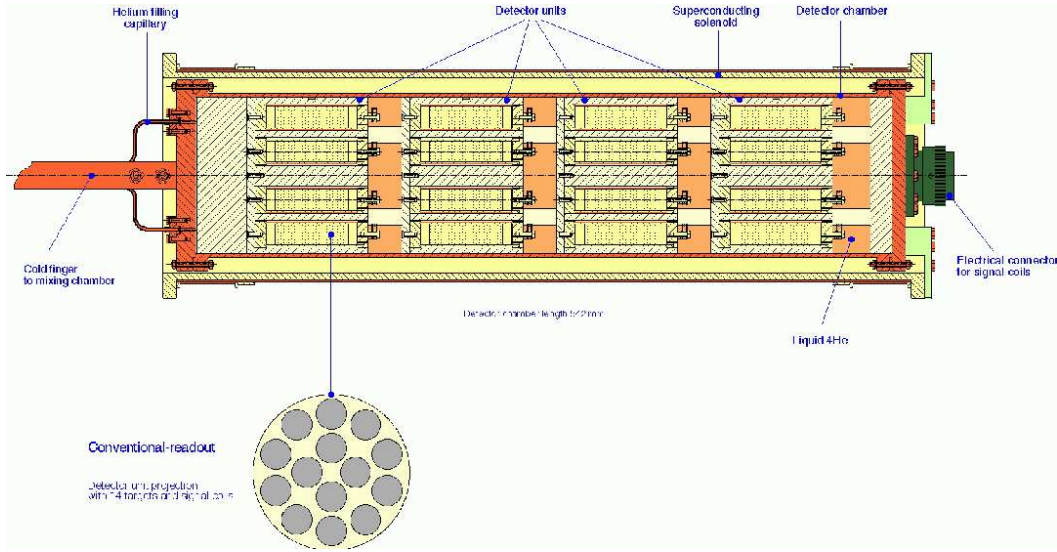


Fig. 2. ORPHEUS detector chamber.

2.2 Electronic readout

ORPHEUS uses a damped resonance parallel RLC circuit to generate a voltage pulse when a flip occurs. The coils have a typical inductance of $L = 10$ mH, cooled shunt resistors of $R = 10$ k Ω , and capacitances $C \approx 1$ nF determined by the combination of cable and input capacitance of the low noise preamplifier. The resonance frequency of the circuit is $f \approx 50$ kHz.

The change in magnetic flux $\Delta\Phi$ caused by a flipping granule of radius r , at applied magnetic field B_a , in the centre of a coil of length l , radius R , and n

windings is,

$$\Delta\Phi = 2\pi B_a n \frac{r^3}{\sqrt{4R^2 + l^2}}. \quad (1)$$

If the flipping time τ is small compared to the characteristic period of the readout circuit ($\tau \ll 2\pi\sqrt{LC}$), the flux variation induces a voltage pulse in the pick-up coil of the form,

$$V(t) = \frac{\Delta\Phi}{\omega LC} e^{-t/2RC} \sin(\omega t) \quad \omega^2 = 1/LC - 1/(2RC)^2. \quad (2)$$

This signal of a few μV is amplified by a factor 10^4 with low noise JFET amplifiers at room temperature. Only 80% of the coil volume is filled with granules in order to get uniform signals within the sensitive volume. A typical granule flip signal ($\phi \approx 36 \mu\text{m}$) fitted to a function of the form (2) can be seen in Fig. 3. The signal to noise ratio is between 10 and 20, depending on the granule size. A detailed description of the readout concept and noise estimations is given in Ref. [14].

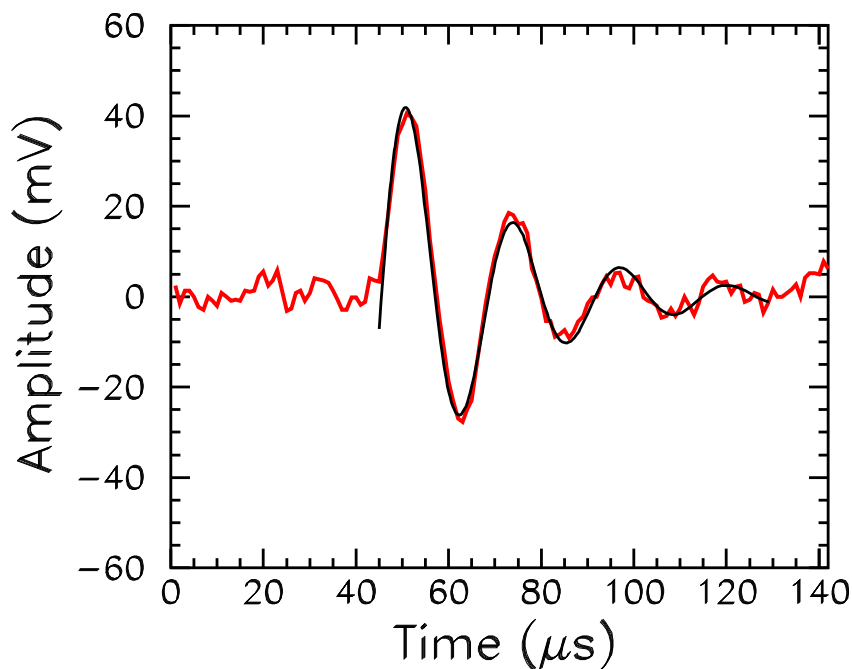


Fig. 3. A typical granule flip signal ($\phi \approx 36 \mu\text{m}$) with its fit.

2.3 Cryogenic system

The detector chamber is kept at a base temperature of 115 mK with a temperature stability of ± 5 mK using a modified Oxford $^3\text{He}/^4\text{He}$ dilution refrigerator of 300 μW cooling power. The cold box consists of concentric copper thermal shields at temperatures of 1.7, 4.5, and 77 K around the detector. Because of the limited vertical space available in the Bern underground facility, a side access of 1.4 m was necessary to connect the mixing chamber of the dilution unit with the detector chamber. All thermal shields of the dilution refrigerator are brought in thermal contact with their corresponding thermal shields on the cold box using flexible bellows. The “L-shaped” configuration poses stringent cooling demands on the dilution refrigerator which were solved by installing two additional cooling jackets, one with liquid N_2 and one with liquid He, in contact with the thermal shields of the cold box through which liquid refrigerants are kept flowing continuously.

The He consumption is typically of 1 l h^{-1} for the dilution refrigerator and 2.6 l h^{-1} for the additional cooling. The total time required to reach the base temperature is approximately 2 weeks. The outer vacuum can and the inner vacuum can operate typically at 10^{-6} mbar.

2.4 Shielding and muon veto

The passive shielding reduces the environmental radioactive flux while the active shielding efficiently vetoes the flux produced by muons from cosmic rays. The passive shielding consists of 15 cm of lead, 4 cm of oxygen free high conductivity copper (OFHC), and 18 cm of boron-doped (5%) polyethylene to moderate and capture environmental neutrons. The detector chamber is made of electroformed copper to guarantee a low radioactivity level. The shielding, resting on wheels, can be opened in two halves to access the detector.

Since ORPHEUS is operated at a shallow depth, active shielding is necessary. Muons are registered by 2 cm thick plastic scintillators (NE 102A) surrounding the passive shielding and analysed off-line to reject signals from the detector chamber in coincidence with the muons within a time window of 15 μs . The plastic scintillators are coupled through wavelengthshifter bars to one or two photomultiplier tubes. The total veto-trigger rate is approximately 5 kHz. At our depth, the expected flux of muon-induced neutrons in 15 cm of lead is 2×10^{-4} n cm^{-2} s^{-1} [15]. We estimate that the muon veto reduces this flux by more than a factor 100.

A series of radiopurity measurements of the detector components were performed with a low-background germanium detector in the underground facil-

Probe	Activities (mBq kg ⁻¹)					
	²³⁸ U	²³² Th	²¹⁰ Pb	¹³⁷ Cs	⁶⁰ Co	⁴⁰ K
Sn granules	<7	<8	<1800	<7	<4	<72
Teflon powder	<9	<11	<70	<10	<9	<108
nylon screws	<14	<14	<70	<13	<7	<139
solenoid wire	<3	<4	<550	<2	<1	<25
Delrin	<10	<12	<91	21 ± 5	<9	<132
OFHC Cu	<82	<136	< 1.2 × 10 ⁴	<86	<65	<1200
connector (280 g)	314±5	295±8	600±15	18±2	24±2	4600±90
Pb shielding	(2 ± 0.4) × 10 ⁵					

Table 1
Sample activities in mBq kg⁻¹ at 95% CL.

ity of the Gotthard tunnel (3000 m.w.e). Several probes were measured for their activity: high purity Sn granules (used in ORPHEUS), Teflon powder (polytetrafluorethylene, PTFE), nylon screws, solenoid wire, Delrin (polyacetal polyoxymethylene, POM), OFHC Cu, a feedthrough connector, and several Pb samples. A summary of the values obtained is shown in Table 1. Not all the samples have the same sensitivities due to differences in the masses of the probes and in measuring times.

A major concern is the activity of the ORPHEUS lead shield. Several probes were measured for their ²¹⁰Pb content by α and γ spectroscopy. It was found that the ORPHEUS lead has on average an activity of ≈ 200 Bq kg⁻¹.

2.5 Data acquisition

To perform off-line pulse shape and background rejection analysis, the phase transition signals are further amplified and digitised in custom-made CAMAC modules or waveform digitisers (WFD). Each WFD has 4 independent channels with differential amplifiers, analog-to-digital converters, memory buffers and voltage comparators providing a trigger signal. Typically 150 points per pulse were digitised at a sampling rate of 1 mega sample per second. A scheme of the readout circuit and data acquisition system can be seen in Fig. 4.

The OR of all 56 comparators is used as an event trigger (see Fig. 4). After each event trigger, the interrupt handling unit (IHU) starts the readout of all

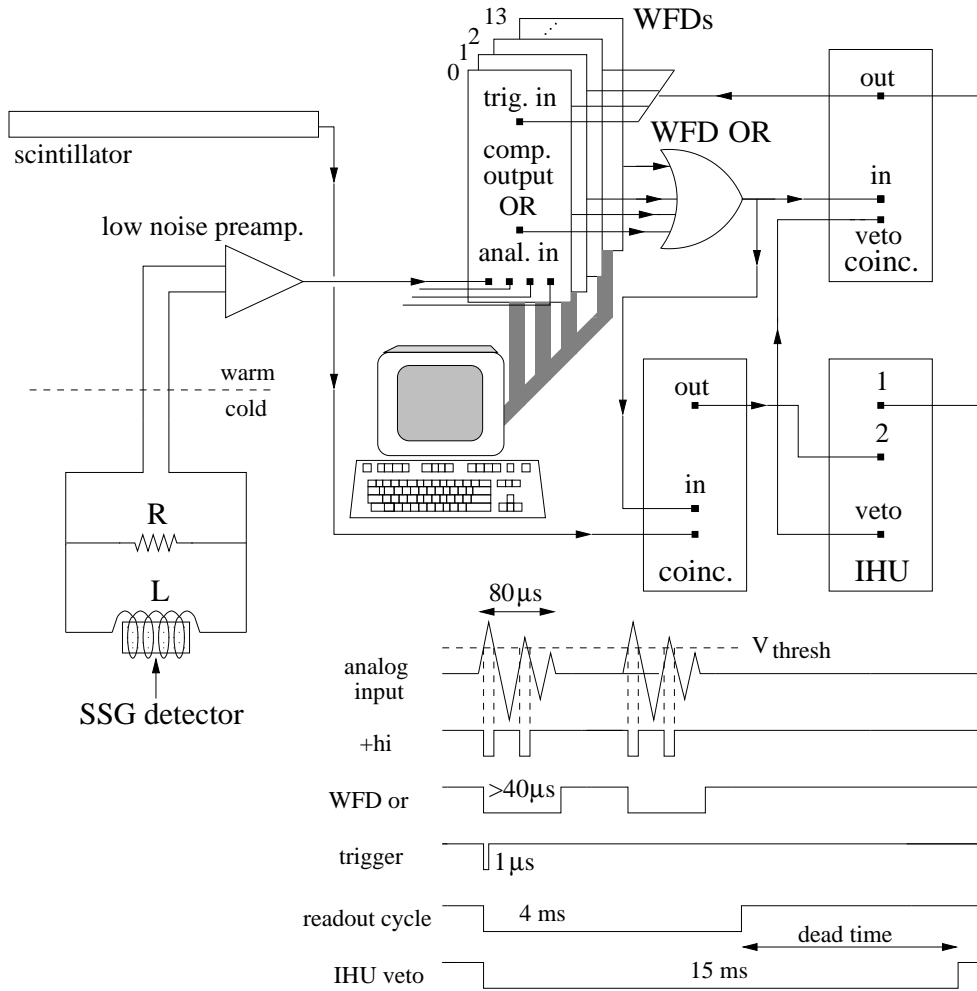


Fig. 4. Readout circuit, data acquisition and timing scheme.

WFD modules and vetoes further triggers during the readout time of 15 ms. The WFDs continue to record the signals during 4.1 ms after the event trigger (memory buffer of 4096 words at $1 \mu\text{s}/\text{word}$), which results in an effective dead time of 11 ms per event. Therefore, at a typical trigger rate in the range of 1 Hz to 10 Hz the dead time was 1% to 11%.

Muon events are rejected off-line if an event is coincident with a plastic scintillator signal within $15 \mu\text{s}$. They are flagged by means of a signal present at the input 2 of the interrupt handling unit (see Fig. 4). Accidental coincidences are also registered measuring the coincidences of the WFD OR with the scintillator signals delayed by $40 \mu\text{s}$.

3 Data taking

We were able to take data continuously during two months in 2002 at a temperature of 170 mK [16,17,18], and during 3 weeks in 2003 at 115 mK. An upgraded acquisition system, as described in the previous section, was implemented in the 2003 run.

The detector threshold is set up by ramping the magnetic field up to a value $H_2 = 285$ G and then lowering it to an operating point H_1 , thus defining the relative magnetic threshold, $h \equiv 1 - H_1/H_2$. Assuming that the entire granule volume needs to be heated (global heating), the magnetic threshold corresponds to an effective energy threshold for each granule size as can be seen in Fig. 5 (see also Eq. A.1). The sensitivity of SSG detectors to minimum-ionising particles [19], X rays [20], and α particles [21,22] has been proved in past experiments. The response of SSG devices to nuclear recoil energies down to 1 keV has been explored irradiating SSG granules with a 70 MeV neutron beam [23].

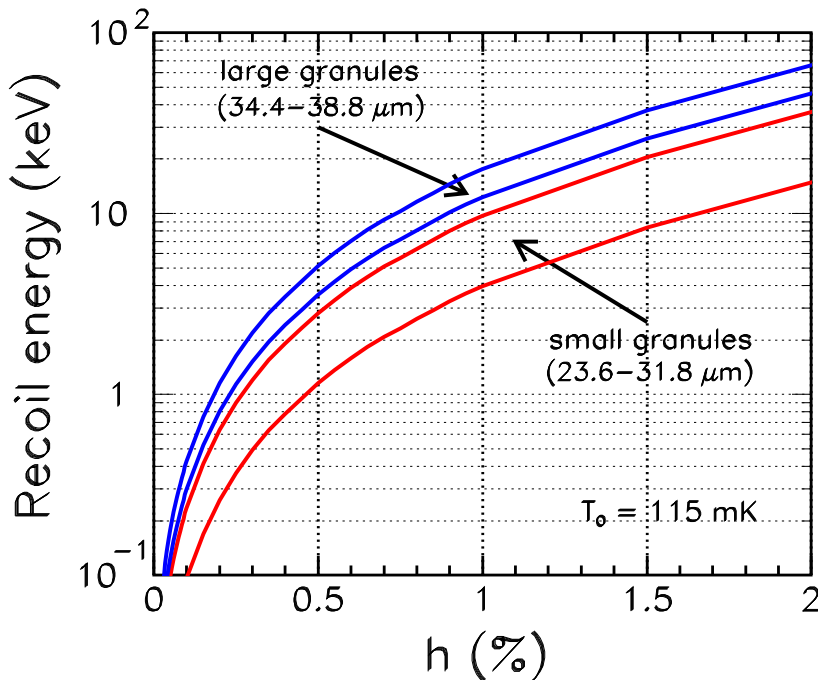


Fig. 5. Estimated granule energy thresholds, assuming global heating model, as a function of magnetic threshold, h , for several granule sizes at 115 mK.

Unfortunately, not all the granules flip at the same magnetic field, but instead they exhibit a distribution of values at which the phase transition occurs, this distribution is the so-called superheating curve. This in turn, has the effect of blurring the effective energy threshold of the detector. A superheating curve characterising our granules, can be measured by slowly increasing the magnetic

field and recording the number of phase transition signals as a function of magnetic field as it is shown in Fig. 6. The superheating spread has a relative width of 22 % at FWHM. The figure also shows, schematically, the values defining the magnetic threshold.

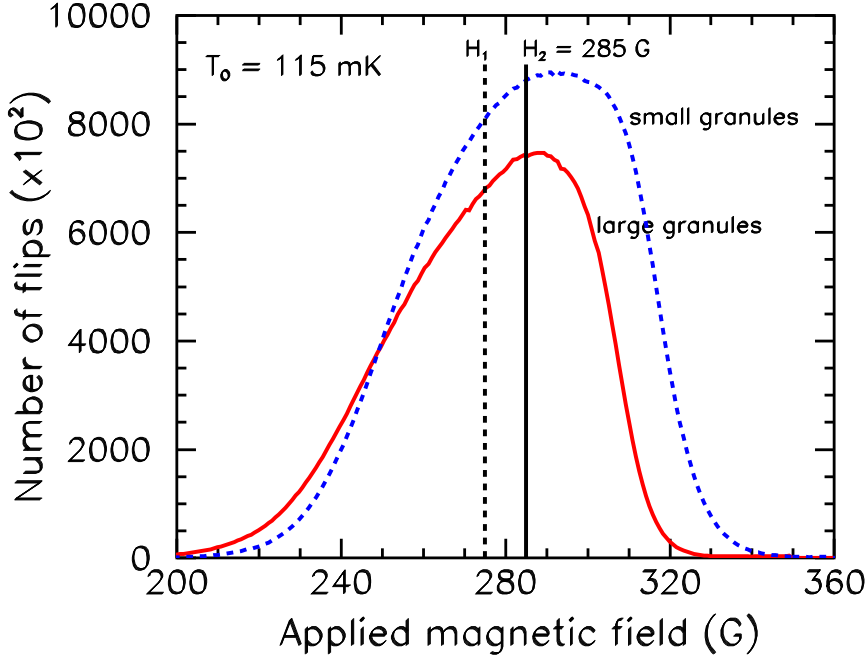


Fig. 6. Superheating field distributions at $T_0=115$ mK.

First results of the 2002 run were published in Refs. [16,17,18]. In the 2003 run, we measured at magnetic thresholds as low as $h = 0.075\%$ and 0.1% . Much lower threshold values were difficult to achieve because magnetic field and temperature instabilities start to be important.

3.1 Data analysis

The raw data of a typical run is depicted in Fig. 7, where a histogram of pulse heights of all digitised pulses in the run is shown. At the lowest amplitudes, the signals due to electronic noise dominate the total rate of $\approx 1 - 10$ Hz. For the large granules (Fig. 7a and Fig. 3) the signals due to single granule flips in a coil (or single flips) are well distinguished from those signals having multiple granule flips in the same coil (double flips or even larger). For the small granules (Fig. 7b) the difference between single and double flips is not so evident due to their wider granule size distribution.

An additional cross-talk noise peak is also seen in Fig. 7a. Noise pulses are characterised by their shape and low amplitudes, while cross-talk signals ex-

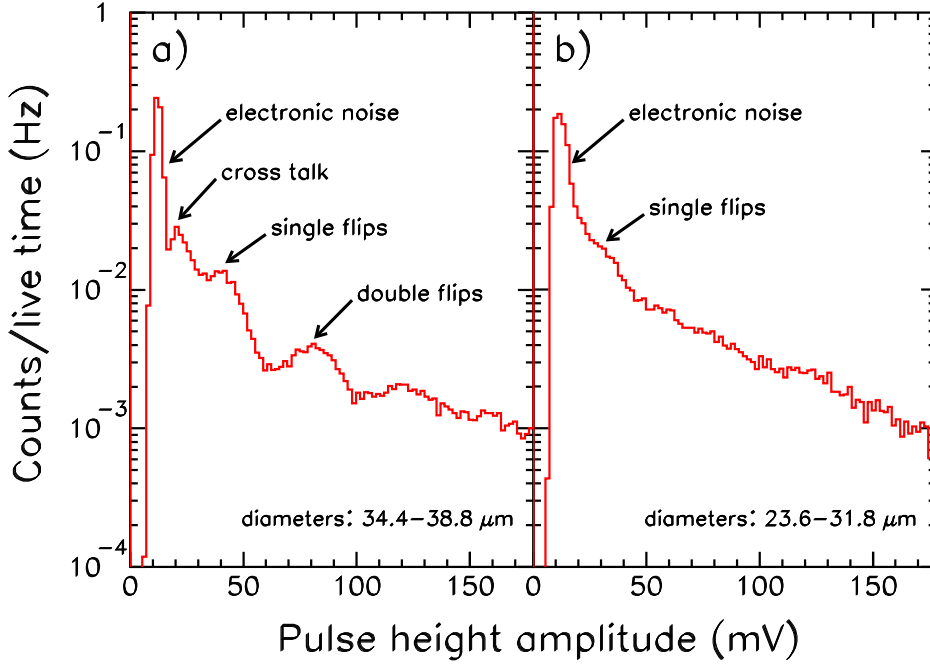


Fig. 7. Pulse height histograms for large, a), and small granules, b).

hibit a polarity opposite to that of regular flips. Cross talk and noisy periods associated with strong vibrations, for instance during N_2 filling, are easily recognised and not considered in further analysis.

3.2 Pulse shape analysis

To efficiently remove the noise pulses from the data, each individual signal is compared off-line to an average standard pulse [17]. A reliable standard pulse is obtained from an average of 500 magnetically induced flips. For each coil this procedure was repeated, but no differences in the standard pulses of different channels were found. The digitised signals are fitted to the standard pulse and only those pulses with a reduced chi square value of $\chi_r^2 \approx 1$ are selected. Figure 8 shows the resulting chi-square distributions for arbitrary samples of flips and noise signals for large, a), and small granules, b). We can appreciate from the figure that a selection criterion of $\chi_r^2 < 2.5$ for the large granules and of $\chi_r^2 < 1.8$ for the small granules still allows a good separation between the two samples even for the small diameter granules. The original histograms of Fig. 7 are shown again in Fig. 9, after the noise and cross-talk pulses have been removed and after a χ_r^2 cut has been applied. Since single flips are not easily distinguished from multiple flips, for small granules, a Gaussian fit to the single flip peak was used to separate singles from multiples.

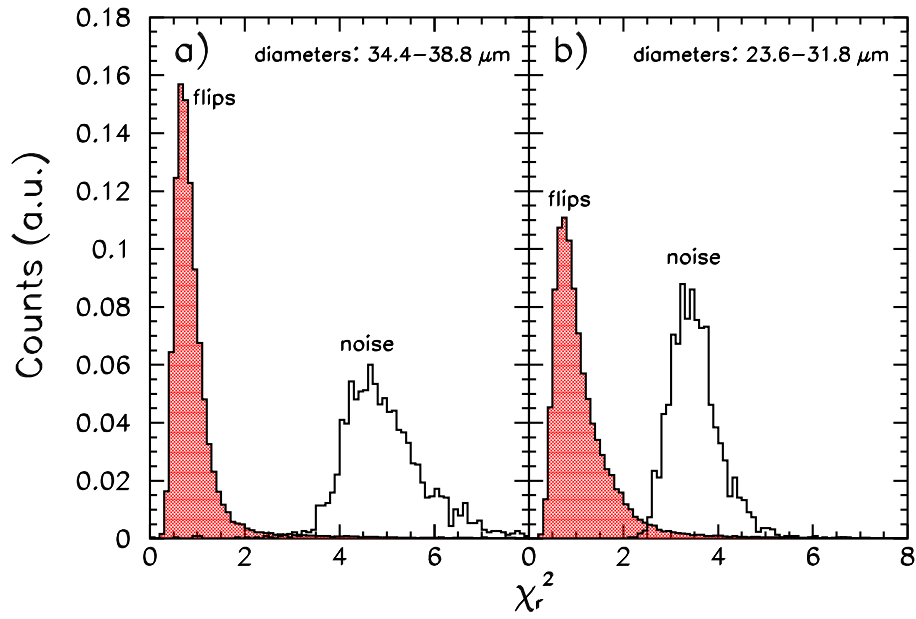


Fig. 8. Reduced chi-square distributions for arbitrary samples of flip and noise pulses of large, a), and small granules, b). Each curve is normalised to a unit area.

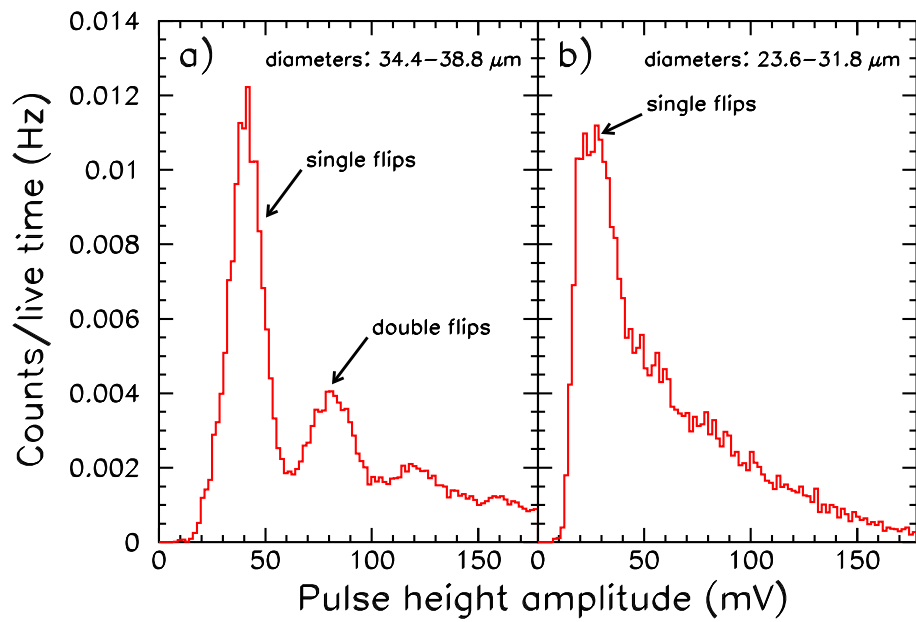


Fig. 9. Filtered pulse height histograms for large, a), and small granules, b).

3.3 Muon rate

The SSG signals induced by muons provide a consistency check for the correct operation of the detector and for the efficiency of the granules for minimum-ionising particles. The event rate of registered SSG signals in coincidence with the muon counters (accidental coincidences subtracted) is shown in Fig. 10 as a function of magnetic threshold. Also shown in the figure are the results of GEANT4 [24] simulations which agree roughly with the expected response of the detector for minimum ionising particles.

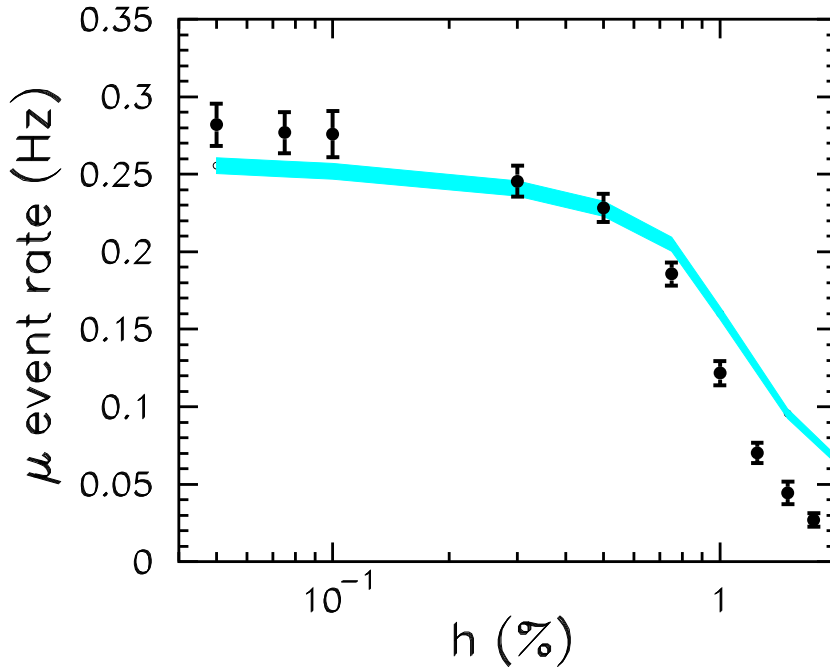


Fig. 10. Event rate of SSG signals in coincidence with the muon counters as a function of magnetic threshold, h . The shaded region shows the results of GEANT4 simulations.

The muon flux intensity per unit area derived from Fig. 10 is in good agreement with an independent previous measurement. This measurement, was done at the underground site with a simpler and smaller scintillator hodoscope arrangement before ORPHEUS was installed.

4 Results

The main result of this experiment relies on efficiently removing background events. While gamma rays and through-going muons are expected to hit more than one granule, ideally, WIMPs are expected to hit only one single granule.

The timing information as well as the coil location of the recorded pulses in each event are used to assess the number of flips per event (multiplicity, M). Fig. 11 shows the rate of events having one single flip in only one coil ($M = 1$) not in coincidence with a muon signal, as a function of detector threshold. As an example, the figure also shows the expected WIMP rates (see Appendix) for two neutralino masses: 20 GeV (solid lines) and 200 GeV (dotted lines). The WIMP cross sections of each curve were chosen so as to give expected rates equal to the upper bounds of the most sensitive points, namely the points with the lowest magnetic thresholds. The error bars are mostly statistical due to the short measuring times. The total exposure for $h = 0.075\%$ threshold, in units of kg.d, is 6.69×10^{-3} .

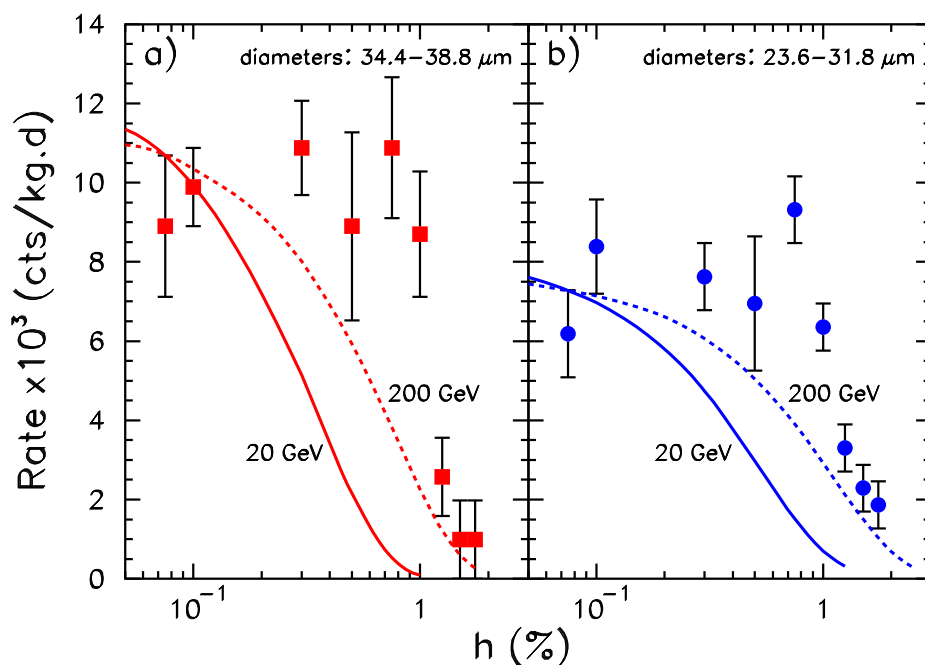


Fig. 11. Rate of flips with multiplicity $M = 1$ not in coincidence with muons for large, a), and small granules, b). Also shown for reference are the expected WIMP rates for masses of 20 GeV (solid lines) and 200 GeV (dotted lines). Expected rates are normalised to the upper bounds of the lowest thresholds.

Neutrons which produce single flip events are an irreducible source of background in this type of experiments. In our underground laboratory, neutrons from the rock with energies between 0.5 – 10 MeV have been measured. The measurements yield a flux of ambient neutrons of $2.4 \times 10^{-4} \text{ n cm}^{-2} \text{ s}^{-1}$. This flux turned out to be of the same order of magnitude as the neutron flux induced by muons being captured in the lead. The 18 cm thick boron-doped polyethylene shielding suppresses the total neutron flux by about two orders of magnitude [25]. Thus, the flux reaching the detector is estimated to be $5 \times 10^{-6} \text{ n cm}^{-2} \text{ s}^{-1}$. In terms of neutrons per kg.d this gives a total neutron background of approximately $10 \text{ n kg}^{-1} \text{ d}^{-1}$.

4.1 Exclusion plots

Comparing the rate of single flips measured with theoretical estimations of the expected spin-independent neutralino rate in our detector, an exclusion plot, like the one shown in Fig. 12 (ORPHEUS line), can be made. The distributions of granule sizes and of superheating fields are taken into account when calculating the expected neutralino rate (see Appendix). Fig. 12 shows the spin-independent neutralino-nucleon elastic cross section versus neutralino mass assuming a local WIMP halo density $\rho_\chi = 0.3 \text{ GeV cm}^{-3}$, an average velocity of the Earth in the halo rest frame $V_E = 243.5 \text{ km s}^{-1}$, and an isothermal spherical halo model with a velocity dispersion $\sigma_v = 270 \text{ km s}^{-1}$. The region above the curve is excluded at a 90% confidence level. For our exclusion plot, we considered the small granule single rates from Fig. 11. Exclusion plots from several other experiments [26,27,28,29,30,31] (labeled lines) are also shown in the figure together with the 3σ annual modulation region, claimed by the DAMA group [32] (grey area). In the constrained minimal supersymmetric extension of the standard model [33], the spin-independent neutralino cross sections lie more than 2 orders of magnitude below the sensitivity of actual experiments.

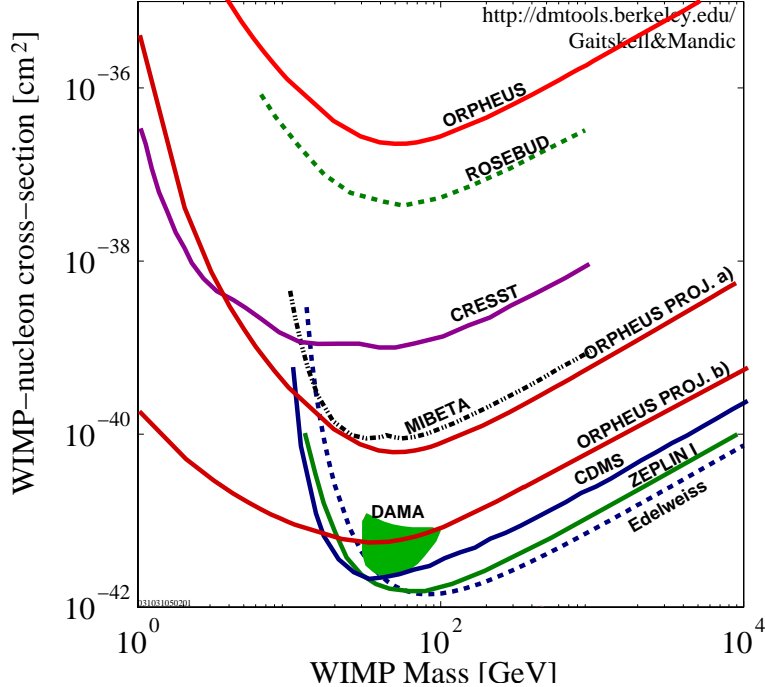


Fig. 12. ORPHEUS spin-independent exclusion plot (ORPHEUS line) together with several other experiments [26,27,28,29,30,31,32] (labeled lines). Projected exclusion plots for ORPHEUS under two different conditions: ORPHEUS PROJ. a) background of $1 \text{ cnt kg}^{-1} \text{ d}^{-1}$ and ORPHEUS PROJ. b) $1 \text{ cnt kg}^{-1} \text{ d}^{-1}$, $10 \mu\text{m}$ granule diameter, and a superheating distribution with FWHM of 1 %.

5 Discussion and outlook

Due to the relatively high background of our experiment the excluded region in Fig. 12 lies above those of other experiments. In the same figure, projected exclusion plots are shown under several assumptions: a) same detector characteristics of the present setup, but a background level of $1 \text{ cnt kg}^{-1} \text{ d}^{-1}$ (attainable at a deeper underground site and with better shielding), b) $1 \text{ cnt kg}^{-1} \text{ d}^{-1}$, smaller granules ($\phi = 10 \text{ }\mu\text{m}$) and a narrower relative spread in the superheating distribution (FWHM = 1 %). Narrower superheating distributions enhance the sensitive mass of the detector and improve at the same time the background rejection capability. The use of smaller granules allows smaller energy depositions to be detected which makes the detector also more sensitive to smaller WIMP masses.

A hint that narrower superheating distribution could be obtained, has been shown by us in Ref. [34] (FWHM $\approx 6 \%$), where a regular array of cylinders, produced with an evaporation method, was used. Also, thermal treatment of the granules with a laser beam has shown to have some effect in reducing the spread of the superheating curve [35]. Detecting single flip signals of smaller granules would require more and smaller pickup coils or a different readout system. The use of superconducting quantum interference devices (SQUID) could offer such a possibility. In the past, already granules of $20\mu\text{m}$ in diameter were measured in a large size prototype [36].

Acknowledgements

We are grateful to T. Ebert and K. U. Kainer from the Technical University of Clausthal (Germany) for the production of the tin granules. We would like to thank M. Hess, S. Lehman, H. Ruetsch and H. U. Schütz for their sustained technical support. We are in particular acknowledging the outstanding efforts in the maintenance and operation of the cryogenics by F. Nydegger. We also would like to thank the Paul Scherrer Institute (Villigen) for providing us with liquid He. This work was supported by the Schweizerische Nationalfonds zur Förderung der wissenschaftlichen Forschung.

A Expected WIMP rates in SSG detectors

Tin granules are type I superconductors with a phase diagram of the form $H(T) \propto [1 - (T/T_c)^2]$ and $T_c = 3.72 \text{ K}$. A granule initially in the superheated superconducting region close enough to its phase transition boundary, say at

(T_o, H_o) , requires only a small temperature increase, $\Delta T = T_f - T_o$ to become normal. The temperature increase can be produced by a WIMP interacting with a granule of radius r_g and depositing an energy,

$$E_t = \frac{4\pi r_g^3}{3} \int_{T_o}^{T_f} C_V(T) dT, \quad (\text{A.1})$$

which represents the minimum deposited energy required to induce a flip. At low enough temperatures, the specific heat of the superconducting granules is dominated by its lattice contribution, $C_V(T) = \beta(T/\theta_D)^3$, where $\theta_D = 195$ K is the Debye temperature for tin and $\beta = 12\pi^4 R/5$, $R = 8.314$ J mol⁻¹ K⁻¹. We see therefore that SSG acts as a threshold detector and that its sensitivity depends on the granule size, working temperature, and distance to the phase transition boundary.

WIMPs of mass m_χ and velocity v elastically scattered off a nucleus of mass m_N can impart to it a recoil energy $E = \mu^2 v^2 (1 - \cos \theta) / m_N$, where μ is the reduced mass of the WIMP-nucleus system and θ the scattering angle in the centre of mass system. The expected WIMP recoil spectrum is given in [7],

$$\frac{dR}{dE} = \frac{\sigma_o \rho_\chi}{2\mu^2 m_\chi} F^2(E) \int_{v_{min}}^{v_{max}} \frac{f(v)}{v} dv, \quad (\text{A.2})$$

where σ_o is the total elastic cross section at zero momentum transfer, ρ_χ is the local halo density of WIMPs, $F^2(E)$ the nuclear form factor, and $f(v)$ the velocity distribution of the WIMPs in the halo for an observer on the Earth. v_{min} is the minimum velocity which contributes to the recoil energy E , namely, $v_{min} = \sqrt{m_N E / 2\mu^2}$, and $v_{max} = 570$ km s⁻¹ the escape velocity from the halo.

The ORPHEUS detector is made of a collection of granules each being sensitive to a slightly different energy due to the spread in their superheating fields. The superheating distribution, dN_{sh}/dH , measured experimentally in section 3, is therefore equivalent through relation (A.1) to a distribution of threshold energies, dN_{sh}/dE_t . The expected number of flips in our detector, R , is thus given by the convolution of the expected integral rate with the distribution of threshold energies, which in turn can be related to the superheating distribution,

$$R_{th} = \int_0^{E_f} \frac{dN_{sh}}{dE_t} \left(\int_{E_t}^{E_{max}} \frac{dR}{dE} dE \right) dE_t = \int_0^{E_{max}} \frac{dR}{dE} \left(\int_{H_o}^{H(E)} \frac{dN_{sh}}{dH} dH \right) dE. \quad (\text{A.3})$$

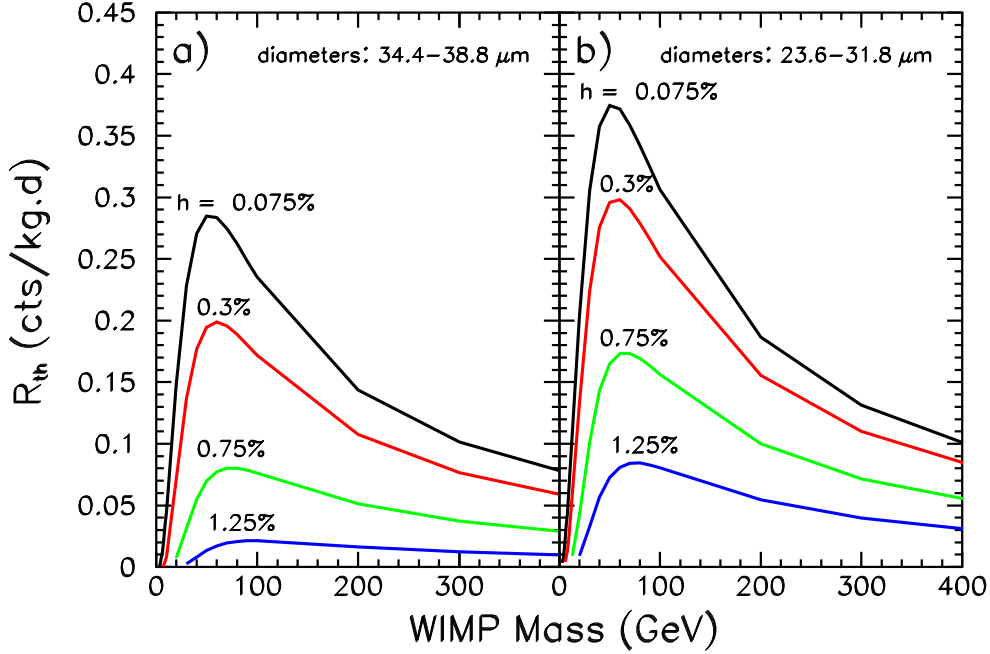


Fig. A.1. Expected WIMP rates as a function of WIMP mass and several detector thresholds, h for large, a), and small granules, b). A temperature of 115 mK and a WIMP–nucleon cross section $\sigma_{\chi p} = 10^{-41} \text{ cm}^2$ have been assumed.

We parametrise the higher fields part of the superheating distribution of Fig. 6 using a Gaussian distribution which is simpler to integrate. We also take into account the fact that the granules have a Gaussian distribution of sizes. Considering all this, Fig. A.1 shows the expected rate of WIMP events in our detector for large and small granules, for different magnetic thresholds h , for a given WIMP–nucleon cross section, $\sigma_{\chi p} = 10^{-41} \text{ cm}^2$ and as a function of WIMP mass. These expected WIMP rates can be directly compared with our experimental results (see Fig. 11).

References

- [1] D. N. Spergel et al., *Astrophys. J. Suppl.* 148 (2003) 175.
- [2] S. Perlmutter et al., *Astrophys. J.* 483 (1997) 565.
- [3] A. G. Riess et al., *Astron. J.* 116 (1998) 1009.
- [4] M. Colless et al., *MNRAS* 328 (2001) 1039.
- [5] M. Tegmark et al., [astro-ph/0310723](https://arxiv.org/abs/astro-ph/0310723).
- [6] H. Hoekstra, H. Yee, M. Gladders, *Astrophys. J.* 577 (2002) 595.

- [7] G. Jungman, M. Kamionkowski, K. Griest, *Phys. Rep.* 267 (1996) 195.
- [8] J. Ellis et al., *Phys. Lett. B* 565 (2003) 176.
- [9] J. Ellis et al., *Phys. Rev. D* 62 (2000) 075010.
- [10] M. Ablanalp et al., *Nucl. Instr. Meth. A* 370 (1996) 227.
- [11] A. Drukier and L. Stodolsky, *Phys. Rev. D* 30 (1984) 2295.
- [12] K. Pretzl, *Part. World* 6 (1990) 153.
- [13] K. Pretzl, *J. Low Temp. Phys.* 93 (1993) 439.
- [14] K. Borer and M. Furlan, *Nucl. Instr. Meth. A* 365 (1995) 491.
- [15] A. Da Silva et al., *Nucl. Instr. Meth. A* 354 (1995) 553.
- [16] G. Czapek et al., *Nucl. Phys. B (Proc. Suppl.)* 110 (2002) 106.
- [17] K. Borer et al. in: *Proceedings of the 4th International Workshop on the Identification of Dark Matter*, York, England, 2002, N. J. C. Spooner and V. Kudryavtsev eds. (World Scientific, Singapore, 2003) p. 332.
- [18] K. Borer et al., *Nucl. Instr. Meth. A* 520 (2004) 112.
- [19] C. Czapek et al., *Nucl. Instr. Meth. A* 306 (1991) 572.
- [20] L. Gonzalez–Mestres and D. Perret–Gallix, *Proceedings of the Workshop on Low Temperature Detectors*, Ringberg Castle, Germany, 1987, K. Pretzl, N. Schmitz and L. Stodolsky eds. (Springer–Verlag, Berlin, 1987) p. 9.
- [21] K. Pretzl et al., *Proceedings of the Workshop on Low Temperature Detectors*, Ringberg Castle, Germany, 1987, K. Pretzl, N. Schmitz and L. Stodolsky eds. (Springer–Verlag, Berlin, 1987) p. 30.
- [22] M. Frank et al., *Nucl. Instr. Meth. A* 287 (1990) 583.
- [23] M. Ablanalp et al., *Nucl. Instr. Meth. A* 360 (1995) 616.
- [24] S. Agostinelli et al., *Nucl. Instr. Meth. A* 506 (2003) 250; GEANT4 Web page: <http://cern.ch/geant4>.
- [25] V. A. Kudryavtsev et al., *Proceedings of the 4th International Workshop on the Identification of Dark Matter*, York, England, 2002, N. J. C. Spooner and V. Kudryavtsev eds. (World Scientific, Singapore, 2003) p. 477.
- [26] A. Benoit et al., *Phys. Lett. B* 545 (2002) 43.
- [27] R. Luscher, *astro-ph/0305310*.
- [28] D. S. Akerib et al., *Phys. Rev. D* 68 (2003) 082002.
- [29] S. Pirro et al., *Proceedings of the 4th International Symposium on Sources and Detection of Dark Matter in the Universe*, Marina del Rey, California, (2000), p. 420.

- [30] F. Probst et al., Nucl. Phys. B (Proc. Suppl.) 110 (2002) 67.
- [31] S. Cebrian et al., Astropart. Phys. 15 (2001) 79.
- [32] R. Bernabei et al., Phys. Lett. B 480 (2000) 23.
- [33] J. Ellis et al., Phys. Lett. B 481 (2000) 304.
- [34] S. Casalbuoni et al., Nucl. Instr. Meth. A 459 (2001) 469.
- [35] S. Calatroni et al., Nucl. Instr. Meth. A 444 (2000) 285.
- [36] B. van den Brandt et al., Nucl. Phys. B (Proc. Suppl.) 70 (1999) 101.